MNRAS 000, 1–5 (2022) Preprint 14 June 2022 Compiled using MNRAS LATEX style file v3.0

Constraining the Evolution of Dwarf Galaxies with Chemical Abundances

James W. Johnson,[1,2]★ Charlie Conroy,[3] Benjamin D. Johnson,[3] Phillip A. Cargile,[3] et al. (?)

[1] *Department of Astronomy, The Ohio State University, 140 W. 18th Ave., Columbus, OH, 43210, USA*
[2] *Center for Cosmology and Astroparticle Physics (CCAPP), The Ohio State University, 191 W. Woodruff Ave., Columbus, OH, 43210, USA*
[3] *Center for Astrophysics | Harvard & Smithsonian, 60 Garden Street, Cambridge, MA, 02138, USA*

Accepted XXX; Received YYY; in original form ZZZ

ABSTRACT

We develop a Bayesian method for fitting one-zone models of galactic chemical evolution to observed stellar abundances and ages. We demonstrate the accuracy of this method by means of mock data samples, for which we are able to recover the known values of evolutionary parameters with accuracy and precision consistent with random processes. Our tests indicate the measrement precision and sample size are of comparable importance in establishing the precision of best-fit parameters, while stellar age information plays a significantly weaker role. We find that known parameters of a mock sample's evolutionary history, including the infall timescale and the duration of star formation, are accurately recovered even in the absence of age information. We apply this method to the Gaia-Sausage-Enceladus and the Sagitarrius dwarf Spheroidal using data observed with the H3 survey. Our characterization of the Gaia-Sausage-Enceladus achieves $\chi^2_{\rm dof} = 1.2$, and the duration of star formation that we derive from chemistry alone is consistent with directage constraints. This method is based on the treatment of stellar abundances in as a one-zone model of galactic chemical evolution sampled according to an inhomogeneous poisson point process. It requires no binning of the data, and should be extensible to other models which predict evolutionary tracks in some observed space (e.g. stellar isochrones and stellar streams).

Key words: methods: numerical – galaxies: abundances – galaxies: evolution – galaxies: star formation – galaxies: stellar content

1 METHODS

• We are interested in applying one-zone GCE models to dwarf galaxies and determining best-fit parameters. We begin by providing background on one-zone models, and then we select a parametrization from which we draw a fiducial mock stellar sample. We then use these data to introduce our fitting method.

1.1 One-Zone Models of Galactic Chemical Evolution

• The fundamental assumption of one-zone models is that newly produced metals mix instantaneously throughout the star forming gas reservoir. This approximation is valid as long as the mixing time-scale is negligible compared to the depletion time-scale (i.e. the average time an fluid element remains in the ISM before getting incorporated into new stars or ejected in an outflow). Based on the observations of Leroy et al. (2008), Weinberg, Andrews & Freudenburg (2017) calculate that characteristic depletion times can range from ∼500 Myr up to ∼10 Gyr for conditions in typical star forming disc galaxies. With the short length-scales and turbulent velocities of dwarf galaxies, instantaneous mixing should be a good approximation.

– If there's an observational reference of metal-mixing in the dwarf galaxy regime - specifically if the scatter in the [α/Fe]-[Fe/H] plane is dominated by observational uncertainty - Evan Kirby would probably be the one to know about it. If not, this would be a good thing to call out as a good observational test of the validity of the one-zone approximation.

• The assumption of instantaneous mixing eliminates the need for spacial information, reducing GCE to a system of coupled integro-differential equations which can be solved numerically.

1.1.1 Inflows, Outflows, Star Formation, and Recycling

• At a given moment in time, gas is added to the interstellar medium (ISM) via inflows and recycled stellar envelopes and is taken out of the ISM via outflows and new stars. This gives rise to the following differential equation describing the evolution of the gas-supply:

$$\dot{M}_{\rm g} = \dot{M}_{\rm in} - \dot{M}_{\star} - \dot{M}_{\rm out} + \dot{M}_{\rm r}, \tag{1}$$

where $\dot{M}_{\rm in}$ is the infall rate, $\dot{M}_{\star}$ is the star formation rate (SFR), $\dot{M}_{\rm out}$ is the outflow rate, and $\dot{M}_{\rm r}$ is the return of stellar envelopes from previous generations of stars.

– We relate the SFR to the gas supply by introducing the "star formation efficiency (SFE) timescale":

$$\tau_{\star} \equiv \frac{M_{\rm g}}{\dot{M}_{\star}}, \tag{2}$$

This quantity is often referred to as the "depletion time" in the observational literature (e.g. Tacconi et al. 2018). This nomenclature,

★ Contact e-mail: johnson.7419@osu.edu

taken from Weinberg et al. (2017), is based on its inverse $\tau_\star^{-1}$ often being referred to as the SFE itself because it describes the *fractional* rate at which some ISM fluid element is forming stars.

– There are various prescriptions for outflows in the literature. Some authors (e.g. Andrews et al. 2017; Weinberg et al. 2017) assume a linear proportionality between the two:

$$\dot{M}_{\rm out} \equiv \eta \dot{M}_\star. \tag{3}$$

Recently, de los Reyes et al. (2022) constrained the evolution of the Sculptor dwarf spheroidal galaxy with a linear proportionality between the SFR and the SN rate $\dot{N}_{\rm II} + \dot{N}_{\rm Ia}$. Kobayashi, Karakas & Lugaro (2020) developed a model in which outflow-driving winds develop in the early phases of the Milky Way's evolution, but die out on some timescale as the Galaxy grows. For modelling the Milky Way, some authors neglect outflows, arguing that they do not signicantly alter the chemical evolution of the disc (e.g. Spitoni et al. 2019, 2021). In our mock sample and in our fits to the GSE and the Sagitarrius dSph, we assume the linear proportionality given by equation (3). Our fitting routine, however, is easily extended to the parametrization of de los Reyes et al. (2022), and if outflows are to be neglected, one can simply take $\eta = 0$ in their fit.

– The recycling rate $\dot{M}_{\rm r}$, in general, depends on the stellar IMF (e.g. Salpeter 1955; Miller & Scalo 1979; Kroupa 2001; Chabrier 2003), the initial-final remnant mass relation (e.g. Kalirai et al. 2008), and mass-lifetime relation (e.g. Larson 1974; Maeder & Meynet 1989; Hurley, Pols & Tout 2000). A single stellar population returns some fraction of its initial mass r back to the ISM according to:

$$r(\tau) = \frac{\int_{m_{\rm to}(\tau)}^{u} (m - m_{\rm rem}) \frac{dN}{dm} dm}{\int_{l}^{u} m \frac{dN}{dm} dm} \tag{4}$$

where l and u are the lower and upper mass limits of star formation, respectively, $m_{\rm to}(\tau)$ is the turnoff mass of a stellar population of age τ, $m_{\rm rem}$ is the mass of a remnant left behind by a star of initial mass m, and dN/dm is the adopted IMF. Under this prescription, the recycling rate from *many* stellar populations, taking into account the full SFH, is given by:

$$\dot{M}_{\rm r} = \int_0^T \dot{M}_\star(t) \dot{r}(T - t) dt \tag{5}$$

where T is the time in the model. Due to the steep nature of the mass-lifetime relation, the recycling rate is dominated by young stellar populations. Weinberg et al. (2017) demonstrate that it is sufficiently accurate in one-zone models to assume that some fraction $r_{\rm inst}$ of a stellar population's initial mass is returned to the ISM immediately (see their Fig. 7; they recommend $r_{\rm inst} = 0.4$ for a Kroupa 2001 IMF, and $r_{\rm inst} = 0.2$ for a Salpeter 1955 IMF). Although it is simpler to assume $\dot{M}_{\rm r} = r_{\rm inst} \dot{M}_\star$, numerical integration of equations (4) and (5) is easy, and `VICE` already does it, so we stick with that.

– Weinberg et al. (2017) demonstrate that $\tau_\star$ and η determine the first-order details of the gas-phase evolutionary track in the [α/Fe]-[Fe/H] plane (see their Fig. 2). With low $\tau_\star$ (i.e. high SFE), nucleosynthesis is fast because star formation is fast, and a higher metallicity can be obtained before the onset of SN Ia than in lower SFE models. For this reason, $\tau_\star$ plays the dominant role in shaping the position of the knee in the [α/Fe]-[Fe/H] plane. As the galaxy evolves, it approaches a chemical equilibrium in which newly produced metals are balanced by the loss of metals to outflows and new stars. Controlling the strength of the sink term of outflows, η plays the dominant role in shaping the late-time equilibrium abundance of the model, which high outflow models (i.e. high η) predicting lower equilibrium abundances than their weak outflow counterparts. For observed data, the shape of the track itself directly constrains these parameters. The detailed form of the SFH has minimal impact on the shape of the tracks; rather, that information is encoded in the density of points along the evolutionary track and in the stellar metallicity distribution functions (MDFs).

1.1.2 Core Collapse Supernovae

• Massive stars, their winds, and their supernovae enrich the ISM on short timescales due to their short lifetimes. As long as the relevant timescales for galaxy evolution are significantly longer than the lifetimes of massive stars, it is adequate to approximate this nucleosynthetic material as ejected instantaneously following a single stellar population's formation. This implies a linear relationship between the CCSN enrichment rate and the SFR:

$$\dot{M}_{\rm x}^{\rm CC} = y_{\rm x}^{\rm CC} \dot{M}_\star \tag{6}$$

where $y_{\rm x}^{\rm CC}$ is the IMF-averaged fractional net yield from massive stars. In parameterizing this term with an IMF-averaged yield, we ipmlicitly assume that the stellar mass is sufficiently high such that stochastic sampling of the IMF is an insignificant effect.

1.1.3 Type Ia Supernovae

• Unlike CCSN enrichment, SN Ia enrichment can occur on delay timescales of a Gyr or more. In general, the enrichment rate can be expressed as an integral over the SFH weighted by the delay-time distribution (DTD):

$$\dot{M}_{\rm x}^{\rm Ia} = y_{\rm x}^{\rm Ia} \frac{\int_0^{T - t_{\rm D}} \dot{M}_\star(t) R_{\rm Ia}(T - t) dt}{\int_0^\infty R_{\rm Ia}(t) dt}, \tag{7}$$

where $R_{\rm Ia}(t)$ is the DTD itself. By comparing the cosmic SFH (e.g. Madau & Dickinson 2014) with the cosmic SN Ia rate, the cosmic SN Ia DTD appears consistent with a uniform t^{-1} power-law (e.g. Maoz & Mannucci 2012; Maoz, Mannucci & Brandt 2012; Graur & Maoz 2013). Following Weinberg et al. (2017), we take a $t^{-1.1}$ power-law DTD with a minimum delay-time of $t_{\rm D} = 150$ Myr.

• In general, the mass of some element x in the ISM is also affected by outflows, recycling, star formation, and infall. The enrichment rate can be calculated by simply adding up all of the source terms and subtracting the sink terms:

$$\dot{M}_{\rm x} = \dot{M}_{\rm x}^{\rm CC} + \dot{M}_{\rm x}^{\rm Ia} - Z_{\rm x} \dot{M}_\star - Z_{\rm x} \dot{M}_{\rm out} + \dot{M}_{\rm x,r}, \tag{8}$$

where the rate of return of the element x from recycled stellar envelopes can be computed by weighting the integral in equation (5) by $Z_{\rm x}(t)$. If there is metal-rich infall, this equation picks up the additional term $Z_{\rm x,in} \dot{M}_{\rm in}$ quantifying that, although here we assume that infall is pristine.

1.1.4 Nucleosynthetic Yields

• In general, nucleosynthetic yields are degenerate with the outflow mass loading factor η. We quantify this is in more detail in

Table 1. The known parameters of the one-zone model from which we generate our mock stellar samples.

Parameter	Description	Value
$\tau_{\rm in}$	e-folding timescale of the infall history	2 Gyr
η	Outflow mass-loading factor ($\eta \equiv \dot{M}_{\rm out}/\dot{M}_\star$)	10
$\tau_\star$	SFE timescale ($\tau_\star \equiv M_{\rm g}/\dot{M}_\star$)	15 Gyr
$\tau_{\rm tot}$	Duration of star formation	10 Gyr
$y_{\rm Fe}^{\rm CC}$	IMF-averaged fractional net Fe yield from CCSNe	0.0008
$y_{\rm Fe}^{\rm Ia}$	IMF-averaged fractional net Fe yield from SN Ia	0.0011

Appendix X, simply noting there that the two are simply the dominant source and sink terms, and as such, high-yield high-outflow models generally have a low-yield low-outflow counterpart that predicts a similar chemical evolution. In order to break this degeneracy, only one number setting the absolute scale is required. Here, we simply set the alpha element yield to $y_\alpha^{\rm CC} = 0.01$. This value is somewhat informed by nucleosynthesis theory in that massive star evolutionary models (e.g. Sukhbold et al. 2016; Limongi & Chieffi 2018; Nomoto, Kobayashi & Tominaga 2013) typically predict $y_{\rm O}^{\rm CC} = 0.005 - 0.015$ (see discussion in, e.g., Weinberg et al. 2017; Johnson & Weinberg 2020), but is otherwise intended to be a round number from which our best-fit values affected by this degeneracy can simply be scaled up or down.

- We let our Fe yields $y_{\rm Fe}^{\rm CC}$ and $y_{\rm Fe}^{\rm Ia}$ be free parameters. With this approach, we implicitly fit the height of the [α/Fe] plateau as well as the Fe yield ratio $y_{\rm Fe}^{\rm CC}/y_{\rm Fe}^{\rm Ia}$.
- In general, nucleosynthetic material is also expelled by asymptotic giant branch (AGB) stars (e.g. Cristallo et al. 2011, 2015; Ventura et al. 2013; Karakas & Lugaro 2016; Karakas et al. 2018). Here we are interested primarily in α and Fe-peak elements, elements whose AGB star yields are negligible compared to their SN yields (e.g. Johnson 2019). We therefore omit discussion of AGB star nucleosynthesis here, but we note that our fitting method described in § 1.3 is easily extensible to include an AGB star enrichment channel. Mathematical details of how this is implemented in `VICE` can be found in Johnson & Weinberg (2020), Johnson et al. (2022), and in the `VICE` science documentation.[1]

1.2 A Fiducial Mock Sample

- We use our parametrization of one-zone GCE models described in § 1.1 to set up an underlying model from which mock samples can be drawn; we then use a fiducial mock sample to describe our fitting method in § 1.3 and explore variations in, e.g., sample size and precision.
- We take an exponential infall history described by

$$\dot{M}_{\rm in} \propto e^{-t/\tau_{\rm in}} \tag{9}$$

with $\tau_{\rm in} = 2$ Gyr and an initial gas mass of 0. The overall normalization of the infall history is irrelevant because mass information cancels in one-zone models when you compute abundances. We additionally select $\tau_\star = 15$ Gyr and $\eta = 10$ with the thought that slow star formation and strong outflows would mimic the evolution seen in a typical field dwarf galaxy. We set the onset of star formation $\tau = 13.2$ Gyr ago, allowing ~0.5 Gyr between the Big Bang and the first stars. We evolve this model for 10 Gyr (i.e. the exact ages of the youngest stars in the mock sample are $\tau = 3.2$ Gyr).
- YIELDS

[1] https://vice-astro.readthedocs.io/en/latest/science_documentation/index.html

- One-zone models produce stellar populations rather than individual stars, so if a mock sample of individual stars is to be obtained, we must sample from the underlying population. Higher mass stellar populations have proportionally more stars than lower mass stellar populations, so we take the probability of sampling to be proportional to the mass of a population. In the interest of mimicing typical observational samples for local group dwarfs, we take $N = 500$ stars with abundance uncertainties of σ[α/Fe] = σ[Fe/H] = 0.05. 100 of these stars have age information with an uncertainty of $\sigma \log_{10}$(age) = 0.1.
- We illustrate this sample in Fig. 1. This sample shows a "knee" in the [α/Fe]-[Fe/H] diagram near [Fe/H] ~-2.3 and an equilibrium abundance near [Fe/H] ~-0.3, but due to the declining nature of the SFH, most of the stars form in the [Fe/H] ~-1 and [α/Fe] ~+0.2 region of chemical space.

1.3 The Fitting Method

- Here we present our method for applying one-zone GCE models to a series of observed abundances and determining the best-fit values. The generic statistical problem at play here is the *inhomogeneous poisson point process* (IPPP). By applying the principles of an IPPP to models which produces tracks in some observed space, we can infer the best-fit parameters given some set of noisy observables in that space. Such models arise not only in the context of chemical evolution as in this work, but also in stellar streams and color-magnitude diagrams (i.e. stellar isochrones). This approach should therefore be extensible to these topics as well.
- Our approach makes the following assumptions regarding the track and the data:

1. The track is infinitely thin. In the absence of observational errors, all of the data would fall perfectly on a line in J-dimensional space.
2. The density *along* the track changes slowly relative to the observational uncertainties.
3. The observational uncertainties on the data are described by a multivariate Gaussian.
4. All of the data are associated with the model.
5. The sample selection is not a function of the observables (though this can be relaxed; see discussion on weights below).

- For a given data sample $\mathcal{D}$, the goal is to find the model $\mathcal{M}$ predicted by a set of parameters θ which maximizes the *posterior probability* $L(\mathcal{M}|\mathcal{D})$. In practice, however, best-fit values for θ are obtained by maximizing the *likelihood function* $L(\mathcal{D}|\mathcal{M})$ describing the probability of observing the data $\mathcal{D}$ given the model $\mathcal{M}$. Bayes' Theorem relates the two according to:

$$L(\mathcal{M}|\mathcal{D}) = \frac{L(\mathcal{D}|\mathcal{M})L(\mathcal{M})}{L(\mathcal{D})} \tag{10}$$

where $L(\mathcal{M})$ is the likelihood of the model (known as the *prior*) and $L(\mathcal{D})$ is the likelihood of the data (known as the *evidence*). The evidence is an overall constant of normalization, but the prior can influence the best-fit values determined by folding in any existing information on the model parameters. In general, it is common to assume a "flat" (or "uniform") prior when no additional information is available, and therefore $L(\mathcal{M}|\mathcal{D}) \approx L(\mathcal{D}|\mathcal{M})$.
- In this context, the goal is to combine the likelihoods for N discrete observations and compute a single likelihood for a given track. As long as each datum is independent of the rest of the sample, the total likelihood can be expressed as the product of the likelihood

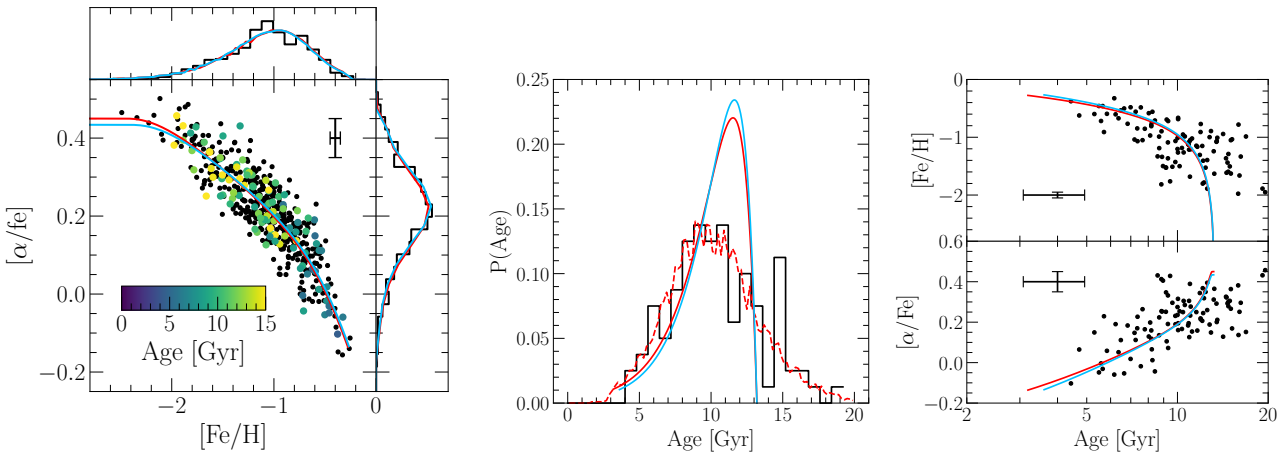

Figure 1. Left: Our fiducial mock sample in the [α/Fe]-[Fe/H] plane. There are $N = 500$ stars with abundance uncertainties of $\sigma([\text{Fe/H}]) = \sigma([\alpha/\text{Fe}]) = 0.05$ as indicated by the errorbar. $N = 100$ of the stars have age information available with an artificial uncertainty of $\sigma(\log_{10}(\text{age})) = 0.1$ as indicated by the colorbar. The red line denotes the evolutionary track in the gas-phase from the one-zone model that generated the mock. On the top and right, we show the marginalized distributions in [α/Fe] and [Fe/H], with red lines denoting the known distribution. **Center**: The mock (black, binned) and known (red) age distributions. The dashed red line indicates the age distribution that is obtained by sampling $N = 10^4$ rather than $N = 500$ stars and assuming the same age uncertainty of $\sigma(\log_{10}(\text{age})) = 0.1$. **Right**: The age-[Fe/H] (top) and age-[α/Fe] (bottom) relation for the mock sample, with artificial uncertainties denoted by the error bars on each panel. The red lines denotes the known relations for the gas-phase.

of each individual datum $\mathcal{D}_i$:

$$L(\mathcal{D}|\mathcal{M}) = \prod_i L(\mathcal{D}_i|\mathcal{M}) \tag{11a}$$

$$\implies \ln L(\mathcal{D}|\mathcal{M}) = \sum_i \ln L(\mathcal{D}_i|\mathcal{M}) \tag{11b}$$

• Computing the likelihood of observing the datum $\mathcal{D}_i$ given some model M is non-trivial because $\mathcal{D}_i$ came from an unknown location along the track. We therefore marginalize $L(\mathcal{D}_i|M)$ over the entirety of $\mathcal{M}$ by integrating the likelihood of a particular observed data point along the entire track. In practice, models will sample the track at some set of K points $\mathcal{M} = \{\mathcal{M}_1, \mathcal{M}_2, \mathcal{M}_3, ..., \mathcal{M}_K\}$, allowing the $L(\mathcal{D}_i|\mathcal{M})$ to be expressed as a summation over all model points $\mathcal{M}_j$:

$$L(\mathcal{D}_i|\mathcal{M}) = \sum_j L(\mathcal{D}_i|\mathcal{M}_j). \tag{12}$$

There are two important factors which additionally influence $L(\mathcal{D}_i|\mathcal{M}_j)$:

1. The inherent density of objects at the point $\mathcal{M}_j$. In the context of chemical evolution, this is directly related to the star formation rate. If the SFR is high at a time j, then it is proprtionally more likely that the datum $\mathcal{D}_i$ is associated with the model point $\mathcal{M}_j$ than at another point in time when the SFR is lower. In the context of, e.g., stellar isochrones and color-magnitude diagrams, this is related to the IMF.

2. The selection function of the sample at the point $\mathcal{M}_j$. If the survey design is such that different regions of the track are sampled more deeply than others, this will be reflected in the distribution in the observed space. In the context of chemical evolution, this can happen by proxy of selection choices in, e.g., stellar age, luminosity, or color.

Because of these factors directly influencing the likelihood function, it is crucial to introduce weights which scale as the product of these two effects:

$$w_j \propto \mathcal{S}(\mathcal{M}_j)\dot{M}_{\star,j} \tag{13}$$

where $\mathcal{S}(\mathcal{M}_j)$ is the selection function of the sample at the point $\mathcal{M}_j$ along the track and $\dot{M}_{\star,j}$ is the model-predicted SFR at time j.

• If the uncertainties of the datum $\mathcal{D}_i$ are adequately described by a multivariate Gaussian, then with the proper weighting, $L(\mathcal{D}_i|\mathcal{M}_j)$ can be expressed as a classical $L \propto e^{-\chi^2/2}$ expression:

$$\chi^2 = \Delta_{ij} C_i^{-1} \Delta_{ij}^T \tag{14}$$

where C_i^{-1} is the inverse covariance matrix associated with the datum $\mathcal{D}_i$ and $\Delta_{ij} = \mathcal{D}_i - \mathcal{M}_j$ is the vector difference between the datum and a given point along the track.

• Combining equations (11b), (12), (13), and (14) results in the following expression for the likelihood function of the data $\mathcal{D}$ given the track $\mathcal{M}$:

$$\ln L(\mathcal{D}|\mathcal{M}) = \sum_i \ln\left(\sum_j w_j \exp\left(\frac{-1}{2}\Delta_{ij} C_i^{-1} \Delta_{ij}^T\right)\right), \tag{15}$$

where the summations are taken over the entirety of the track and the entirety of the data.

• In detail, an IPPP requires the sum of the weights $\sum_j w_j$ to be subtracted from $\ln L(\mathcal{D}|\mathcal{M})$. The purpose of this term is such that tracks which go "too far" in the observed space are penalized for predicting data in regions where there are none. However, in the context of chemical evolution, the weights are derived from the SFH of the model. For the models we consider here, the normalization of the SFH is inconsequential to the model predictions (i.e. a model with the SFH amplified by 10^6 at all times but otherwise the same evolutionary parameters would predict the same evolution in [Fe/H] and [α/Fe]). For this reason, it is essential that $\sum_j w_j$ not impact the inferred value of $\ln L(\mathcal{D}|\mathcal{M})$. We therefore set $\sum_j w_j = 1$ always, and tracks which extend too far in chemical space are penalized by contributing a *fractional* weight far from the observed points, thereby increasing χ^2. However, for applications of this method in which the sum of the weights is *not* inconsequential to the likelihood function, this additional term in equation (15) must be included. (It may be worthwhile to include an appendix in which we demonstrate the validity of this approach).

- Although there are variety of ways in which one could construct the likelihood function $L(\mathcal{D}|\mathcal{M})$, in the present paper we use the Markov Chain Monte Carlo (MCMC) method. Despite being more computationally expensive than, e.g., maximum likelihood estimates, MCMC methods offer a more generic solution than by sampling tails and multiple modes of the likelihood distribution that would otherwise be missed by assuming Gaussianity. With this choice, this method should be applicable to additional data sets perhaps described by GCE models with different parametrizations.
- We use the `emcee` software (Foreman-Mackey et al. 2013) to run our MCMC fits. At each step in parameter space, `emcee` makes a call to `VICE` to compute the predicted abundances for that selection of parameters. We then compute the likelihood function $L(\mathcal{D}|\mathcal{M})$ according to equation (15) and let `emcee` take care of the rest.
- In § 1.4, we apply this method to our fiducial mock sample and discuss how the accuracy and precision of the recovered known parameters is affected by sample size, precision, and the availability of age information.

1.4 Mock Sample Fits

REFERENCES

Andrews B. H., Weinberg D. H., Schönrich R., Johnson J. A., 2017, ApJ, 835, 224
Chabrier G., 2003, PASP, 115, 763
Cristallo S., et al., 2011, ApJS, 197, 17
Cristallo S., Straniero O., Piersanti L., Gobrecht D., 2015, ApJS, 219, 40
de los Reyes M. A. C., Kirby E. N., Ji A. P., Nuñez E. H., 2022, ApJ, 925, 66
Foreman-Mackey D., Hogg D. W., Lang D., Goodman J., 2013, PASP, 125, 306
Graur O., Maoz D., 2013, MNRAS, 430, 1746
Hurley J. R., Pols O. R., Tout C. A., 2000, MNRAS, 315, 543
Johnson J. A., 2019, Science, 363, 474
Johnson J. W., Weinberg D. H., 2020, MNRAS, 498, 1364
Johnson J. W., Weinberg D. H., Vincenzo F., Bird J. C., Griffith E. J., 2022, arXiv e-prints, p. arXiv:2202.04666
Kalirai J. S., Hansen B. M. S., Kelson D. D., Reitzel D. B., Rich R. M., Richer H. B., 2008, ApJ, 676, 594
Karakas A. I., Lugaro M., 2016, ApJ, 825, 26
Karakas A. I., Lugaro M., Carlos M., Cseh B., Kamath D., García-Hernández D. A., 2018, MNRAS, 477, 421
Kobayashi C., Karakas A. I., Lugaro M., 2020, ApJ, 900, 179
Kroupa P., 2001, MNRAS, 322, 231
Larson R. B., 1974, MNRAS, 166, 585
Leroy A. K., Walter F., Brinks E., Bigiel F., de Blok W. J. G., Madore B., Thornley M. D., 2008, AJ, 136, 2782
Limongi M., Chieffi A., 2018, ApJS, 237, 13
Madau P., Dickinson M., 2014, ARA&A, 52, 415
Maeder A., Meynet G., 1989, A&A, 210, 155
Maoz D., Mannucci F., 2012, Publ. Astron. Soc. Australia, 29, 447
Maoz D., Mannucci F., Brandt T. D., 2012, MNRAS, 426, 3282
Miller G. E., Scalo J. M., 1979, ApJS, 41, 513
Nomoto K., Kobayashi C., Tominaga N., 2013, ARA&A, 51, 457
Salpeter E. E., 1955, ApJ, 121, 161
Spitoni E., Silva Aguirre V., Matteucci F., Calura F., Grisoni V., 2019, A&A, 623, A60
Spitoni E., et al., 2021, A&A, 647, A73
Sukhbold T., Ertl T., Woosley S. E., Brown J. M., Janka H. T., 2016, ApJ, 821, 38
Tacconi L. J., et al., 2018, ApJ, 853, 179
Ventura P., Di Criscienzo M., Carini R., D'Antona F., 2013, MNRAS, 431, 3642
Weinberg D. H., Andrews B. H., Freudenburg J., 2017, ApJ, 837, 183